

Article

# Partial Discharge Detection and Defect Location Method in GIS Cable Terminal

Songyuan Li <sup>1</sup>, Pengxian Song <sup>1</sup>, Zhanpeng Wei <sup>2</sup>, Xu Li <sup>1</sup>, Qinghua Tang <sup>1</sup>, Zhengzheng Meng <sup>1</sup>, Ji Li <sup>3</sup>, Songtao Liu <sup>1</sup>, Yuhuai Wang <sup>4</sup>  and Jin Li <sup>4,\*</sup> 

<sup>1</sup> State Grid Tianjin Electric Power Research Institute, Tianjin 300384, China

<sup>2</sup> Power Cable Company, Tianjin 300300, China

<sup>3</sup> State Grid Tianjin Electric Power Company, Tianjin 300100, China

<sup>4</sup> Key Laboratory of Smart Grid of Education Ministry, School of Electrical and Information Engineering, Tianjin University, Tianjin 300072, China

\* Correspondence: lijn@tju.edu.cn

**Abstract:** The complex structure of gas-insulated switchgear (GIS) cable terminals leads to serious electric field concentration, which is a frequent fault position of a high-voltage cable system. At present, due to the differences in the frequency bands of sensors, various partial discharge detection technologies have certain differences in their scope of application and anti-interference performance, resulting in a low defect detection rate in GIS cable terminals. In this paper, a comprehensive diagnosis scheme is proposed, which integrates transient earth voltage (TEV), ultra-high frequency (UHF), high frequency (HF), and ultrasonic methods. Two abnormal discharge defects of GIS terminals in two 220 kV substations in Tianjin were tracked and monitored, and the joint diagnosis was carried out using the proposed scheme; the type of discharge defect and the phase sequence of the defect were determined, and the UHF was employed to precisely locate and analyze the defect source. Finally, through the disassembly analysis and electric field simulation of the GIS cable terminal, the accuracy and effectiveness of the discharge detection and location method were verified, providing a typical detection demonstration for the defect diagnosis of a GIS cable terminal.

**Keywords:** GIS cable termination; UHF; joint diagnoses; dissection analysis; electric field distribution



**Citation:** Li, S.; Song, P.; Wei, Z.; Li, X.; Tang, Q.; Meng, Z.; Li, J.; Liu, S.; Wang, Y.; Li, J. Partial Discharge Detection and Defect Location Method in GIS Cable Terminal. *Energies* **2023**, *16*, 413. <https://doi.org/10.3390/en16010413>

Academic Editor: Pawel Rozga

Received: 12 November 2022

Revised: 16 December 2022

Accepted: 28 December 2022

Published: 29 December 2022



**Copyright:** © 2022 by the authors. Licensee MDPI, Basel, Switzerland. This article is an open access article distributed under the terms and conditions of the Creative Commons Attribution (CC BY) license (<https://creativecommons.org/licenses/by/4.0/>).

## 1. Introduction

With the rapid development of urban and power grid construction, gas-insulated switchgear and high-voltage cross-linked polyethylene (XLPE) cables have been widely used in the power grid due to their superior electrical performance, compact and economical space requirements, and safe and reliable operation [1–5]. As the connection between the gas-insulated switchgear and the XLPE cable, the GIS cable terminal has a complex composite interface and electric field stress concentration in its interior, which is the weak link and fault-prone part of the cable system [6–10]. In recent years, extreme weather events have occurred more frequently and increased the probability of cable insulation failure [11–14]. Therefore, ensuring the safe and stable operation of the GIS cable terminal is of great significance to the electrical equipment and high-voltage cable line in the substation.

Before an insulation failure of cable terminals occurs, it is usually accompanied by various characteristic information such as electricity, heat, sound, light, moisture and gas changes [15–19]. For information about the different characteristics, current detection technology has derived a variety of detection technologies, such as infrared thermal image detection, ultra-high-frequency (UHF) partial discharge detection, high-frequency partial discharge detection, ultrasonic partial discharge detection, transient earth voltage partial discharge detection, dissolved gas analysis in oil, SF<sub>6</sub> gas state detection, etc., [20–22]. Due to the insulation and sealing of 110 kV and above XLPE cable terminals, there are few

obvious characteristics before failure. The insulation defects inside the cable terminals cause electric field distortion and induce partial discharge, which are accompanied by changes in electrical and acoustic signals. Therefore, the insulation status is mainly judged by the changes in electric and acoustic signals. The effective measurement of the partial discharge of the terminals is the main method for quality control and status detection in the GIS cable terminals in the operating stations [23,24]. Power grid operators at home and abroad have continually explored and applied the pulse current method, broadband electromagnetic coupling method, ultrasonic method and ultra-high frequency detection method and other location methods [25,26]. However, in actual field applications, due to differences in the scope of application, detection sensitivity, anti-interference performance, etc., of the various types of partial discharge detection equipment, as well as different understandings of the structure, performance and testing environment of the tested equipment, the defect detection rates for the GIS cable terminal are low [27].

## 2. Methods

The process of GIS cable terminal partial discharge detection was obtained by integrating the GIS cable terminal structure and various methods, which are shown in Figure 1. Each detailed step and the precautions taken are introduced below.

- (1) TEV and UHF methods are used first to complete a rapid general test, and preliminarily judge whether there is an abnormal signal according to the signals of transient voltage pulse and ultra-high frequency electromagnetic wave. During the general TEV test, the TEV sensor should be put in the middle of the host top to ensure that the contact surface with the equipment is as large as possible.
- (2) If any suspicious abnormal signal is found, the full spectrum detection should be used for retesting and the abnormal TEV signal can be converted into an HF signal.
- (3) Based on the polarity of the three-phase waveform of the abnormal HF signal, the phase source can be determined. During polarity detection and judgment, it should be ensured that all channels use the same cable model (BNC or N type) and the same cable length. The signals of each phase must be triggered separately to judge the possibility of multi-phase (point) discharge.
- (4) If the abnormal signal comes from one phase, the time difference of arrival (TDOA) positioning for the abnormal phase is carried out. If there is no difference in the three-phase signal polarity, the three-phase signal polarity should be compared with that of the grounding wire to determine whether it is from ground grid interference. During TDOA positioning, the length and model of signal line should be consistent. Various amplifiers should be connected to ensure that the signals of each channel are original.
- (5) The TDOA positioning results of the HF, VHF and UHF methods should be comprehensively compared. As the range error of the positioning results may be large, it is recommended to take the local discharge position as  $X = \{0, X_{\Delta t}\}$ . The amplifier must not be connected in this step, otherwise an additional cable length (between the amplifier and the oscilloscope) will be introduced, causing a time-difference calculation error.

Figure 2 presents a typical HF signal polarity diagram of an oil–oil bushing transformer, when the 220 kV C-phase cable terminal was the signal source. The position of HFCT at the grounding wire of the phase A cable terminal on the 220 kV side should be kept unchanged each time (yellow ring). The red arrow represents the high-frequency current flowing from the equipment to the ground, and the blue arrow represents the high-frequency current flowing from the ground to the equipment. The red dotted box of phase A on the 110 kV side shows that two different types of data were collected many times, and the results were not unique.

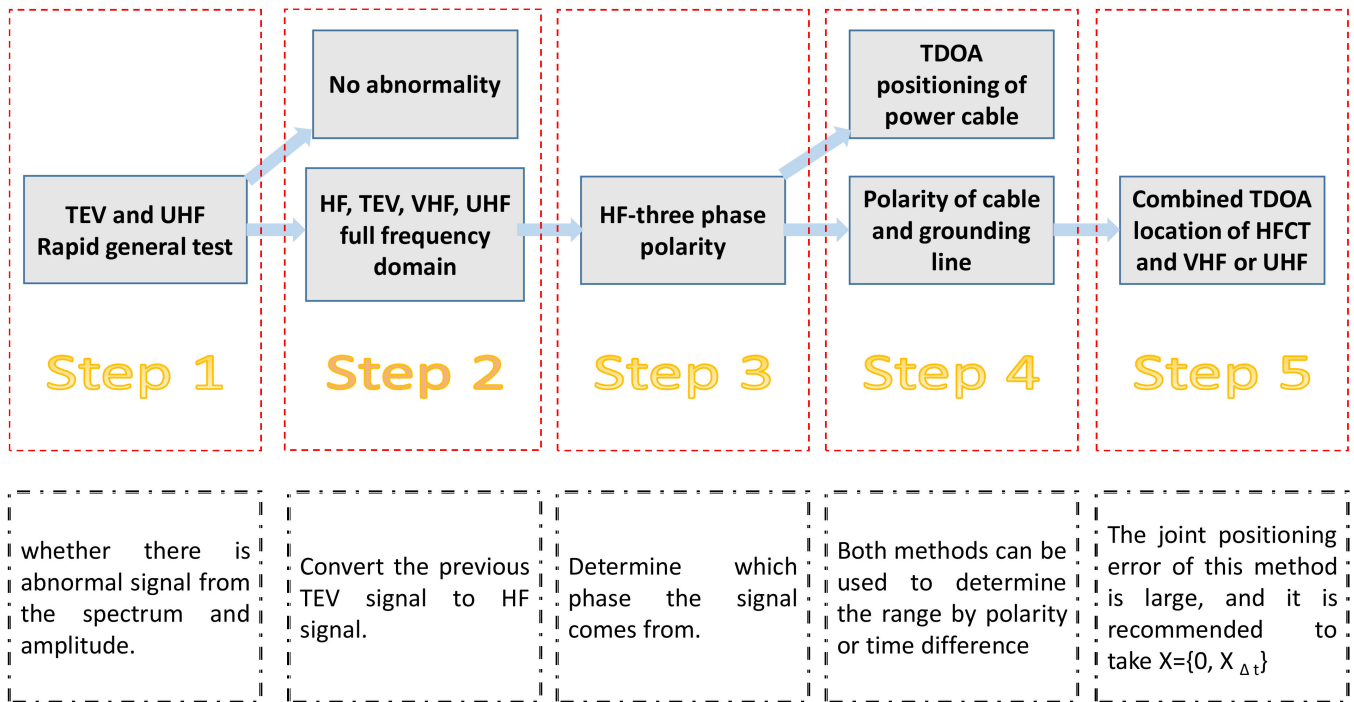


Figure 1. Diagram for the defects detection and location in GIS cable terminal.

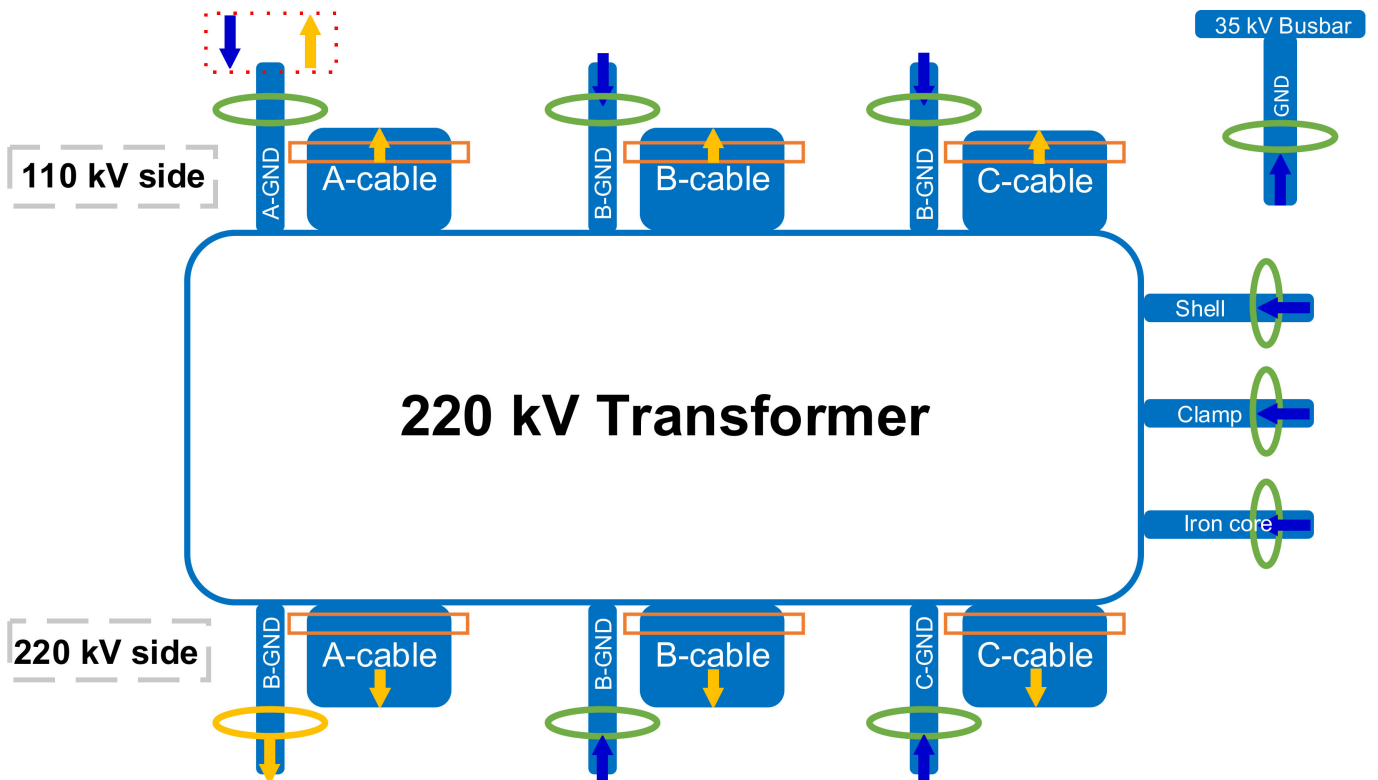


Figure 2. HF signal polarity diagram of oil-oil bushing transformer (220 kV C-phase cable terminal is the signal source).

### 3. Results

#### 3.1. Case 1

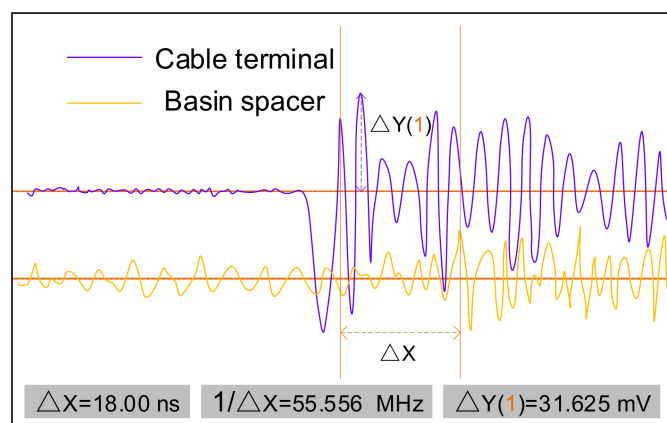
##### 3.1.1. Partial Discharge Characteristics and Location

Five kinds of partial discharge detection methods and decomposition gas detection test were carried out for the 2215 bay of a 220 kV Milan gas-insulated substation in Tianjin City. Table 1 presents the specific test items and test results.

**Table 1.** Test items and related results of 2215 bay of 220 kV Milan Station.

Tests	Results	Remarks
UHV for GIS	Abnormal	Discharge by insulation defects
HV for cable	Normal	
Ultrasonic for GIS	Normal	TDOA and amplitude
TEV	Normal	
PD location	Cable compartment	
Decomposition gas detection	Normal	

An abnormal partial discharge signal was detected at the 2215 bay A-phase cable compartment and basin insulator above the current transformer (CT) upper side, and there was no abnormality at other positions. According to the characteristics of the discharge spectrum, it was judged an insulation discharge. The amplitude at the cable terminal was greater than that at the basin insulator above the CT, and the maximum amplitude was  $-53$  dB. See Figure 3 for the detection location and Table 2 for the typical map.

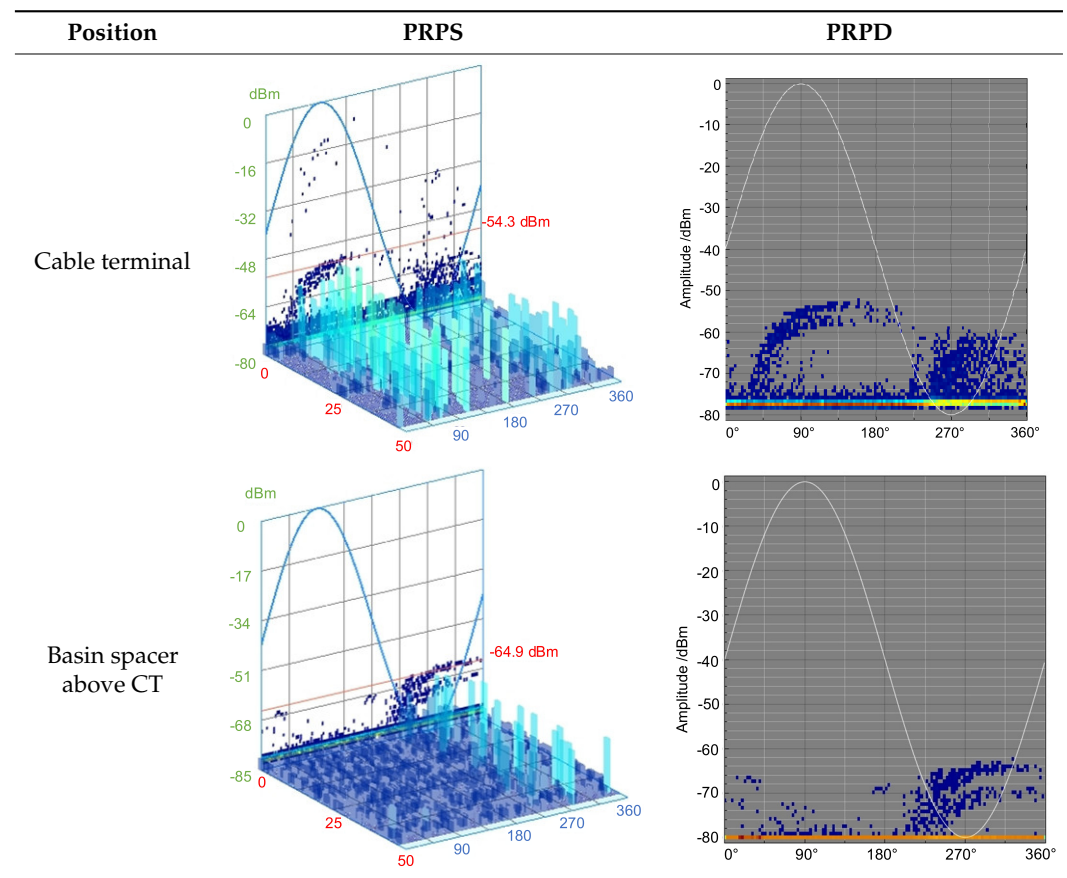


**Figure 3.** Signal diagram of two detection positions in A-phase cable compartment.

In order to accurately locate the defect position of the discharge source, the inspector selected the discharge signal at the basin insulator above the CT side (yellow) and the epoxy resin flange at the cable terminal (purple) for local discharge source location analysis. It is shown in Figure 3 that the rising edge of the yellow signal curve was not obvious due to the small discharge amplitude.

##### 3.1.2. Disassembly Verification

In order to verify the partial discharge detection results in Section 3.1.1., the A-phase cable was taken out of the cable chamber and disassembled to determine the defect location of the A-phase cable. It was found that there was a dark yellow solid substance in the area close to the fracture between the semi-conductive layer and the cable insulation, and the same substance also existed at the corresponding inner position of the stress cone, as shown in Figure 4.

**Table 2.** Typical spectrum of UHF detection in A-phase cable compartment.

(a)

(b)

**Figure 4.** Morphology of the abnormal area of cable terminal. (a) Semi-conductive layer, (b) inside the stress cone.

The dark yellow solid substance was tested by infrared spectrum. The functional group analysis results are shown in Figure 5. The wave numbers  $1261\text{ cm}^{-1}$  represented the Si-CH<sub>3</sub> functional group,  $1095\text{ cm}^{-1}$ ,  $1021\text{ cm}^{-1}$  for Si-O-Si functional group, and  $800\text{ cm}^{-1}$  for CH<sub>3</sub> functional group, which confirmed that the substance was silicone oil. The wave number around  $1681\text{ cm}^{-1}$  represented the carbonyl C=O functional group, which confirmed that the silicone oil had deteriorated.

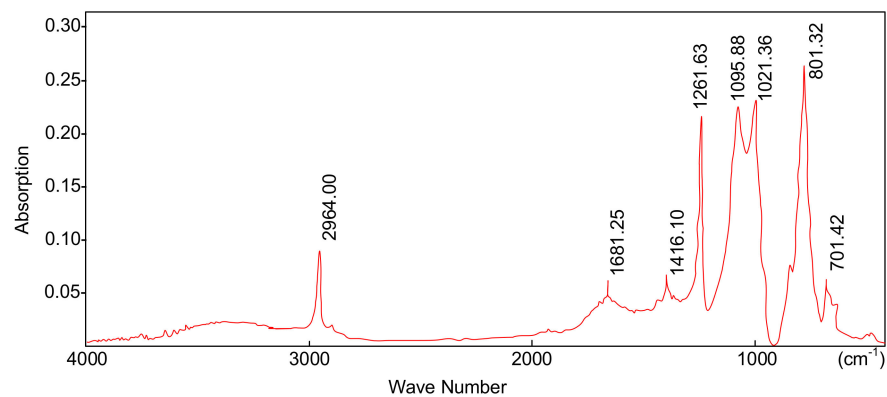


**Figure 5.** Infrared spectral analysis of solid substance.

### 3.2. Case 2

#### 3.2.1. Partial Discharge Characteristics and Location

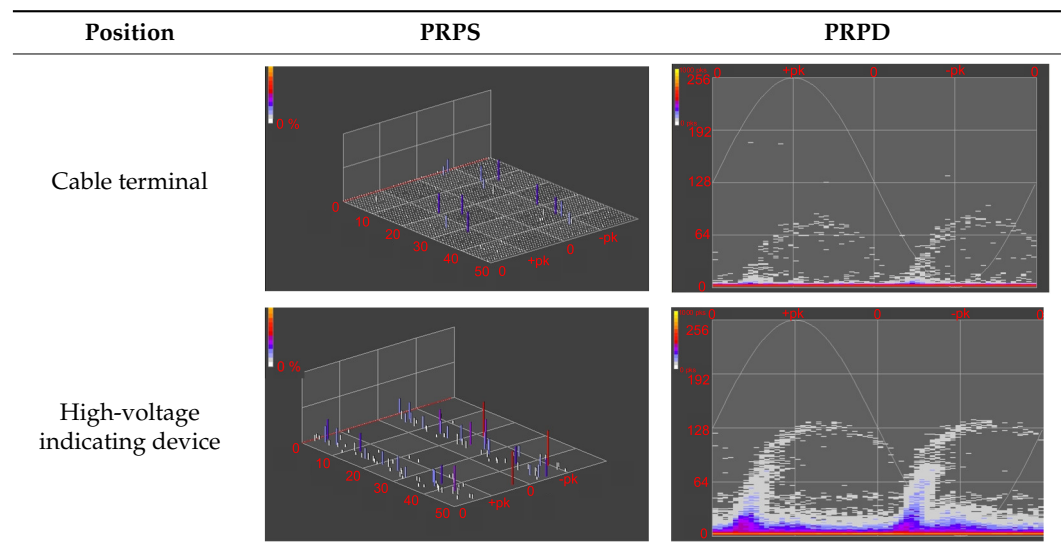
Five kinds of partial discharge detection methods and decomposition gas detection tests were carried out for the 2202 bay of a 220 kV Chuanye gas-insulated substation in Tianjin City. Table 3 presents the specific test items and test results.

**Table 3.** Test items and related results of 2202 bay of 220 kV Chuanye Station.

Tests	Results	Remarks
UHV for GIS	Abnormal	Discharge by insulation defects Interference signal
HV for cable	Abnormal	
Ultrasonic for GIS	Normal	
TEV	Normal	
PD location	Cable compartment	TDOA and amplitude
Decomposition gas detection	Normal	

An abnormal partial discharge signal was also detected at the 2202 bay A-phase cable terminal and high-voltage indicating device of the GIS, and no UHF partial discharge anomaly map was found in the space background, phase B or phase C. It was seen from the results in Table 4 that the discharge pulse had obvious periodicity, large amplitude dispersion and an unstable discharge time interval, so the detection spectrum was similar to that of typical insulation defects.

**Table 4.** Typical spectrum of UHF detection in A-phase cable compartment.



In order to reduce the measurement error, multiple time-delay positioning was carried out. As shown in Figure 6, the green sensor (cable terminal) waveform was always ahead of the purple sensor (high-voltage indicating device) waveform, and the time difference between the two positions was 1.56 ns. It was calculated that the discharge power was located 0.7 m above the bottom flange of the 2202 interval A-phase cable terminal.

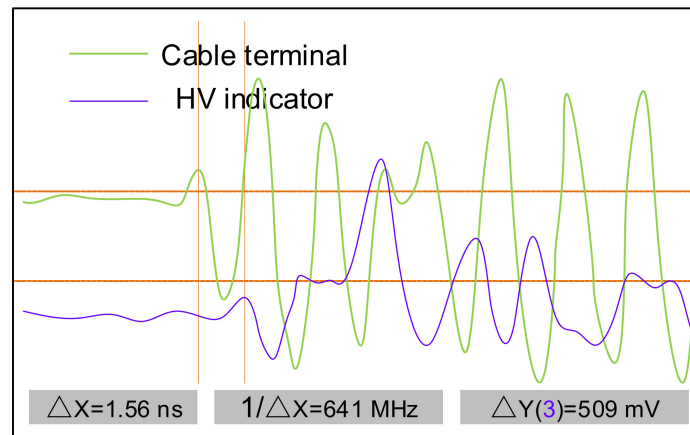


**Figure 6.** Signal diagram of two detection positions in A-phase cable compartment.

### 3.2.2. Disassembly Verification

The A-phase cable terminal was drawn out from the lower end of the cable bin, and no obvious discharge trace was found on the outer surface of the stress cone and epoxy sleeve after careful inspection, as shown in Figure 7. The stress cone was split longitudinally. Through inspection, it was found that there was a 7 cm long crack on the inner surface of the stress cone (6 to 13 cm from the upper end of the stress cone), which was consistent with the detection results of partial discharge.

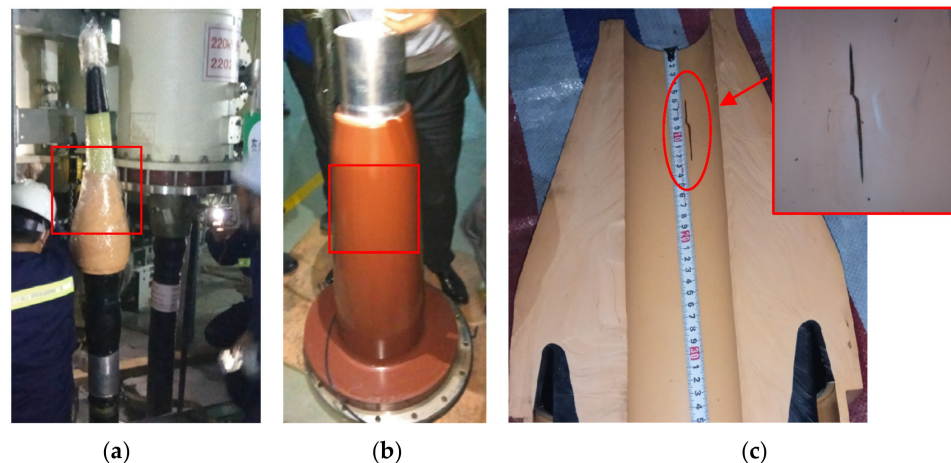


**Figure 7.** Morphology of the disassembled cable terminal. (a) Stress cone and XLPE insulation, (b) epoxy sleeve, (c) crack inside the stress cone.

## 4. Discussion

### 4.1. Electric Field Distribution

The electric field simulation model of the GIS cable terminal was established in the COMSOL software to study the electric field distortion between the semiconductive fracture and the stress cone interface with the deterioration of silicone oil and the presence of air gap or impurities. The rated voltage at the cable conductor was 127 kV and the voltage of the ground flange was set to 0 kV. Under AC voltage, the electric field distribution of the

cable terminal is mainly determined by the relative dielectric constant of the material. The governing equations used in this paper are as follows:

$$\nabla \cdot D = \rho_V \quad (1)$$

$$D = \varepsilon_0 \varepsilon_r E \quad (2)$$

$$E = -\nabla V \quad (3)$$

where  $D$  is the electric displacement vector ( $C/m^2$ ),  $\varepsilon_0$  and  $\varepsilon_r$  are the permittivity of the vacuum and relative permittivity of materials, respectively,  $\rho_V$  is the local charge density ( $C/m^3$ ),  $E$  is the electric field vector ( $V/m$ ), and  $V$  is the potential ( $V$ ).

As shown in Figure 8a, the thickness of the silicon oil coating was set to 0.1 mm. Under normal working conditions, the maximum electric field strength inside the silicon oil coating is 2.56 kV/mm. Under this field strength, there is no possibility of partial discharge inside the cable terminal. In consideration of the irregular impurities in the coated silicone oil, we set different shapes of defects as shown in Figure 8. The results show that the maximum electric field strength in the coated silicone oil was 6.45 kV/mm, which was 252% of the normal working condition. With the electric field distortion, the discharge accident may have been further induced here, causing further deterioration of the silicone oil and insulation failure of GIS cable terminal.

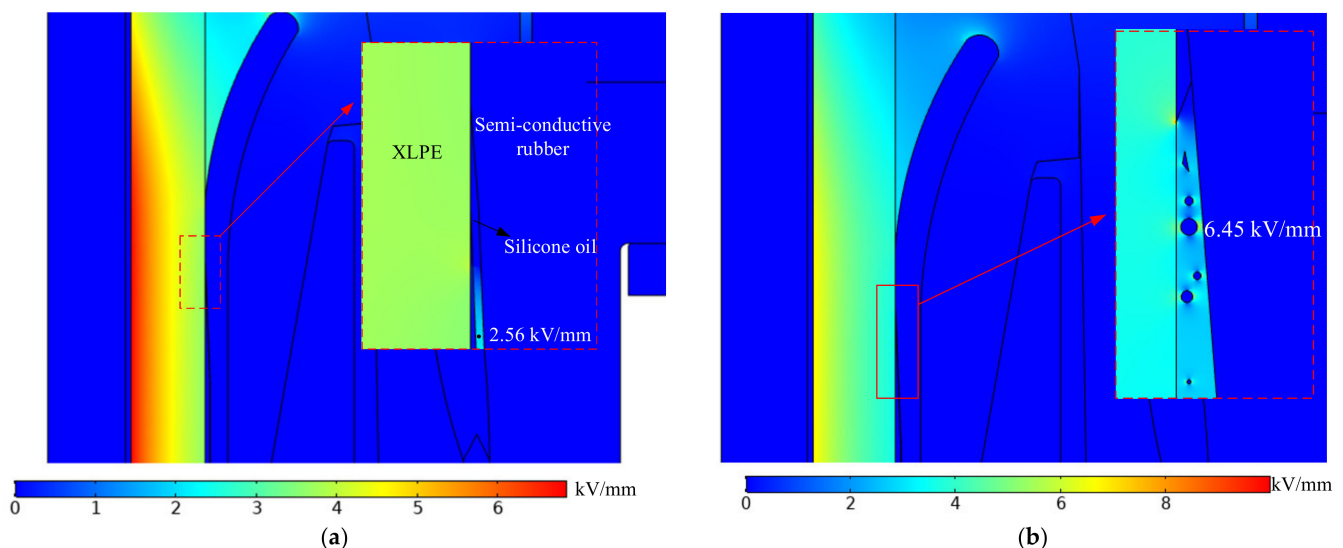


**Figure 8.** Electric field distortion at the interface in GIS cable terminal: (a) without defects, (b) with defects.

#### 4.2. Internal Discharge Development Mechanism

##### 4.2.1. Stage I: Development from Surface Discharge

At the initial stage, there are a lot of burr-like protrusions in the defects of the cable terminal. The discharge channel is short and the discharge amplitude is small. Some discharges are even lower than the detection accuracy of the sensor and are difficult to detect. Under the sinusoidal voltage, when the electric field direction changes, the positive and negative charges show different mobility, the discharge behavior is inconsistent, and the discharge develops toward the ground potential in a single direction, which shows the characteristics of asymmetric positive and negative cycles. At the same time, because the air gap in the early aging period is narrow, the charges accumulated in the air gap dissipate. The discharge repetition rate in the PRPD map is high, but the amplitude is low, and it operates for a long time, which causes these burrs to gradually ablate and smooth.

#### 4.2.2. Stage II: Enhanced Partial Discharge

The discharge further develops and some areas inside the air gap gradually elongate to form a long air gap channel. At this time, the discharge in the air gap is more intense around the terminal of the air gap. The PRPD spectrum showed positive and negative half cycle symmetry. The expansion of the air gap makes it necessary to accumulate more charges before breakdown, and the discharge repetition frequency is relatively reduced. With continuous aging, the occasional large pulse discharge gradually develops into a stable discharge with reduced voltage amplitude but an increased discharge repetition rate.

### 5. Conclusions

According to the detection status of the GIS cable terminals, a comprehensive detection method combining the TEV method and the UHF method was proposed in this paper, and partial discharge detection was carried out at 220 kV GIS cable terminals. The conclusions are as follows:

- (1) A diagnosis scheme suitable for a GIS cable terminal is proposed, which can effectively determine the type and phase sequence of discharge defects, and accurately locate and analyze the defect source at ultra-high voltage.
- (2) The disassembly analysis of the GIS cable terminals showed the accuracy and effectiveness of the discharge defects and positioning methods, which provided a typical detection demonstration for GIS cable terminal-defect diagnosis. However, the sensitivity of this scheme to detect partial discharge at the initial stage of internal terminal faults needs to be improved.
- (3) The electric field distribution of the GIS cable terminal was analyzed by finite element simulation, and the mechanism of the internal fault of the cable terminal was analyzed.

**Author Contributions:** Conceptualization, S.L. (Songyuan Li), P.S. and J.L. (Jin Li); methodology, Z.W.; software, S.L. (Songtao Liu); validation, J.L. (Ji Li), Q.T. and Z.M.; formal analysis, J.L. (Ji Li); investigation, X.L.; resources, S.L. (Songyuan Li) and P.S.; data curation, X.L.; writing—original draft preparation, J.L. (Jin Li) and Y.W.; writing—review and editing, P.S. and X.L.; visualization, X.L.; supervision, Q.T.; project administration, J.L. (Ji Li); funding acquisition, P.S. All authors have read and agreed to the published version of the manuscript.

**Funding:** This research was funded by Science and Technology Project of State Grid Tianjin Electric Power Company (KJ22-1-28).

**Data Availability Statement:** Not applicable.

**Conflicts of Interest:** The authors declare no conflict of interest.

### References

1. Li, J.; Liang, H.; Chen, Y.; Du, B. Promising Functional Graded Materials for Compact Gaseous Insulated Switchgears/Pipelines. *High Volt.* **2020**, *5*, 231–240. [[CrossRef](#)]
2. Zheng, J.; Chen, Z.; Wang, Q.; Qiang, H.; Xu, W. GIS Partial Discharge Pattern Recognition Based on Time-Frequency Features and Improved Convolutional Neural Network. *Energies* **2022**, *15*, 7372. [[CrossRef](#)]
3. Nadolny, Z. Electric Field Distribution and Dielectric Losses in XLPE Insulation and Semiconductor Screens of High-Voltage Cables. *Energies* **2022**, *15*, 4692. [[CrossRef](#)]
4. Bakhshizadeh, M.K.; Vilmann, B.; Kocewiak, Ł. Modal Aggregation Technique to Check the Accuracy of the Model Reduction of Array Cable Systems in Offshore Wind Farms. *Energies* **2022**, *15*, 7996. [[CrossRef](#)]
5. Arsenyev, D.; Dubitsky, S.; Kiesewetter, D.; Malyuin, V. Numerical Simulation and Calculation of Resistance of Laminated Paper-Impregnated Insulation of Power Cables. *Energies* **2022**, *15*, 7403. [[CrossRef](#)]
6. Li, J.; Wang, Y.; Song, P.; Zhu, W.; Liang, H.; Du, B. Dynamic Interface Charge Behaviors in HVDC Cable Terminal Considering Carrier Dynamic Equilibrium. *IEEE Trans. Fundamen. Mater.* **2021**, *141*, 567–573. [[CrossRef](#)]
7. Zhao, X.; Yang, X.; Gao, L.; Li, Q.; Hu, J.; He, J. Tuning the potential distribution of AC cable terminals by stress cone of nonlinear conductivity material. *IEEE Trans. Dielectr. Electr. Insul.* **2017**, *24*, 2686–2693. [[CrossRef](#)]
8. Kim, S.; Lee, D.; Kim, J.; Lee, B. Numerical Analysis of Electric Field Characteristics and Interfacial Pressure of HVDC XLPE Cable Joint Considering Load Cycles. *Energies* **2022**, *15*, 4684. [[CrossRef](#)]

9. Li, J.; Du, B.; Su, J.; Liang, H.; Liu, Y. Surface Layer Fluorination-Modulated Space Charge Behaviors in HVDC Cable Accessory. *Polymers* **2018**, *10*, 500. [[CrossRef](#)]
10. Zhang, Z.P.; Zheng, C.J.; Zheng, M.; Zhao, H.; Zhao, J.K.; Sun, W.F.; Chen, J.Q. Interface Damages of Electrical Insulation in Factory Joints of High Voltage Submarine Cables. *Energies* **2020**, *13*, 3892. [[CrossRef](#)]
11. Li, J.; Liu, S.; Song, P.; Du, B. Solidification Dynamics of Silicone Oil and Electric Field Distribution Within Outdoor Cable Terminations Subjected to Cold Environments. *IEEE Trans. Power Deliv.* **2022**, *37*, 4126–4134. [[CrossRef](#)]
12. Panteli, M.; Mancarella, P. Influence of Extreme Weather and Climate Change on the Resilience of Power Systems: Impacts and Possible Mitigation Strategies. *Electr. Power Syst. Res.* **2015**, *127*, 259–270. [[CrossRef](#)]
13. Panteli, M.; Mancarella, P. Modeling and Evaluating the Resilience of Critical Electrical Power Infrastructure to Extreme Weather Events. *IEEE Syst. J.* **2017**, *11*, 1733–1742. [[CrossRef](#)]
14. Guo, C.; Ye, C.; Ding, Y.; Wang, P. Multi-State Model for Transmission System Resilience Enhancement Against Short-Circuit Faults Caused by Extreme Weather Events. *IEEE Trans. Power Deliv.* **2021**, *36*, 2374–2385. [[CrossRef](#)]
15. Lemke, E. Analysis of the Partial Discharge Charge Transfer in Extruded Power Cables. *IEEE Electr. Insul. Mag.* **2013**, *29*, 24–28. [[CrossRef](#)]
16. Mu, L.; Xu, X.; Xia, Z.; Yang, B.; Guo, H.; Zhou, W.; Zhou, C. Autonomous Analysis of Infrared Images for Condition Diagnosis of HV Cable Accessories. *Energies* **2021**, *14*, 4316. [[CrossRef](#)]
17. Wang, H.; He, C.; Guo, R.; Meng, X.; Yuan, W.; Li, J. Partial Discharge Measurement and Analysis Under Lightning Impulse Superimposed DC Voltage in SF<sub>6</sub> Gas. *High Volt.* **2022**, *7*, 744–752. [[CrossRef](#)]
18. Jiang, J.; Chen, J.; Li, J.; Yang, X.; Albarracín-Sánchez, R.; Ranjan, P.; Zhang, C. Propagation and Localisation of Partial Discharge in Transformer Bushing Based on Ultra-High Frequency Technique. *High Volt.* **2021**, *6*, 684–692. [[CrossRef](#)]
19. Zheng, Q.; Luo, L.; Song, H.; Sheng, G.; Jiang, X. Intelligent Learning Approach for UHF Partial Discharge Localisation in Air-Insulated Substations. *High Volt.* **2020**, *5*, 583–590. [[CrossRef](#)]
20. Xing, C.; Zang, Q.; He, R.; Zhao, J.; Wang, L.; Dai, L.; Shi, R.; Wang, S.; Ma, G. Phase Stability Control of Optical Fiber Partial Discharge Ultrasonic Sensing System. *Sensors* **2022**, *22*, 8495. [[CrossRef](#)]
21. Baug, A.; Choudhury, N.; Ghosh, R.; Dalai, S.; Chatterjee, B. Identification of Single and Multiple Partial Discharge Sources by Optical Method Using Mathematical Morphology Aided Sparse Representation Classifier. *IEEE Trans. Dielectr. Electr. Insul.* **2017**, *24*, 3703–3712. [[CrossRef](#)]
22. Yang, J.; Yan, K.; Wang, Z.; Zheng, X. A Novel Denoising Method for Partial Discharge Signal Based on Improved Variational Mode Decomposition. *Energies* **2022**, *15*, 8167. [[CrossRef](#)]
23. Stone, G.; Cavallini, A.; Behrmann, G. A Review of the History of the Development of Partial Discharge Testing. In Proceedings of the 2022 IEEE Electrical Insulation Conference (EIC), Knoxville, TN, USA, 19–23 June 2022; pp. 85–89.
24. Liu, F.; Ding, D.; Chen, L.; He, L.; Zhu, J.; Ma, Q.; Zhang, H.; Zeng, H. Combined Diagnosis of GIS Cable Termination Based on Partial Discharge Detection with Multi Frequency Band. *High Volt. Appar.* **2020**, *56*, 266–274.
25. Tariq, R.; Alhamrouni, I.; Rehman, A.U.; Tag Eldin, E.; Shafiq, M.; Ghamry, N.A.; Hamam, H. An Optimized Solution for Fault Detection and Location in Underground Cables Based on Traveling Waves. *Energies* **2022**, *15*, 6468. [[CrossRef](#)]
26. Li, G.; Chen, J.; Li, H.; Hu, L.; Zhou, W.; Zhou, C.; Li, M. Diagnosis and Location of Power Cable Faults Based on Characteristic Frequencies of Impedance Spectroscopy. *Energies* **2022**, *15*, 5617. [[CrossRef](#)]
27. Cheng, X.; Tao, S.; Wang, W. The Partial Discharge Detection and Location as Well as Dissection of 110 kV XLPE Cable Terminal. *Proc. CSEE* **2013**, *33*, 226–230.

**Disclaimer/Publisher’s Note:** The statements, opinions and data contained in all publications are solely those of the individual author(s) and contributor(s) and not of MDPI and/or the editor(s). MDPI and/or the editor(s) disclaim responsibility for any injury to people or property resulting from any ideas, methods, instructions or products referred to in the content.